Robust Non-linear Observers for Attitude Estimation on mini UAVs

Robert Mahony and Tarek Hamel

Robert Mahony is with Department of Engingeering, ANU, ACT, 0200, Australia, Robert.Mahony@anu.edu.au.

Tarek Hamel is with I3S-CNRS, Nice-Sophia Antipolis, France, thamel@i3s.unice.fr.

Abstract

A key requirement for the control and navigation of any autonomous flying vehicle is the availability of a robust attitude estimate. Small scale aerial robotic vehicles such as mini or micro aerial vehicles use low-cost lightweight inertial measurement units (characterised by high noise levels and time varying additive biases) and embedded avionics systems that make classical stochastic filter techniques unviable. This chapter proposes a suite of non-linear attitude observers that fuse angular velocity and orientation measurements in an analogous manner to that of a complementary filter for a linear system. By exploiting the natural geometry of the group of rotations an attitude observer is derived that; requires only accelerometer and gyro outputs; is suitable for implementation on embedded hardware; and provides robust attitude estimates as well as estimating the gyro biases on-line. Experimental results from a robotic test-bed and a radio controlled unmanned aerial vehicle are provided to verify the filter performance.

Keywords: Complementary filter, nonlinear observer, attitude estimates, special orthogonal group.

1 Introduction

The last decade has seen an intense world wide effort in the development of mini aerial vehicles (mAV). Such vehicles are characterised by;

small scale (dimensions of the order of 60cm), limited payload capacity, and embedded avionics systems. A key component of the avionics system in a mAV is the attitude estimation subsystem [2,12,30]. Such systems must be highly reliable and have low computational overhead to avoid overloading the limited computational resources available in some applications. Traditional linear and extended Kalman filter techniques [14,3,20] suffer from issues associated with poor modelling of the system (in particular, characterisation of noise within the system necessary for tuning filter parameters) as well as potentially high computational requirements [28,30]. An alternative is to use deterministic complementary filter and non-linear observer design techniques [35,2,1,34]. Recent work has focused on some of the practical issues encountered when data is obtained from low cost inertial measurement units (IMU) [26,1,34,23] as well as observer design for partial attitude estimation [27,21,22]. It is also worth mentioning the related problem of fusing IMU and vision data [16,25,13,7,6] and the problem of fusing IMU and GPS data [24,34]. A key issue in attitude observer design for systems with low-cost IMU sensor units is on-line identification of gyro bias terms. This problem is also important in IMU calibration of attitude observers for satellites [14,8,4,32,17]. An important development that came from early work on estimation and control of satellites was the use of the quaternion representation for the attitude kinematics [29,9,32,31]. The non-linear observer designs that are based on this work have strong robustness properties and deal well with the bias estimation problem [34,32]. The quaternion representation for attitude can provide a significant computational advantage in the implementation of observer algorithms. However, it tends to obscure the underlying geometric structure of the algorithms proposed.

In this chapter, we study the design of non-linear attitude observers on the group of rotations, the special orthogonal group $SO(3)$. We term the proposed observers *complementary filters* because of the similarity of the architecture to that of linear complementary filters, although, for the non-linear case we do not have a frequency domain interpretation. A general formulation of the error criterion and observer structure is described on the Lie-group structure of $SO(3)$. This formulation leads us to define two non-linear observers on $SO(3)$, termed the *direct complementary filter* and *passive complementary filter* [19]. The direct complementary filter corresponds (up to some minor technical differences) to non-linear observers proposed using the quaternion representation [29,32,34]. We do not know of a prior reference for the passive complementary filter. The passive complementary filter has several practical advantages associated with implementation and low-sensitivity to noise. In particular, we show that the

filter can be reformulated in terms of direct measurements from the IMU system, a formulation that we term the *explicit complementary filter* [11]. The explicit complementary filter does not require on-line algebraic reconstruction of attitude, an implicit weakness in prior work on non-linear attitude observers due to the computational overhead of the calculation and poor error characterisation of the constructed attitude. As a result the observer is ideally suited for implementation on embedded hardware platforms. Furthermore, the relative contribution of different data can be preferentially weighted in the observer response, a property that allows the designer to adjust for application specific noise characteristics. Finally, the explicit complementary filter remains well defined even if the data provided is insufficient to algebraically reconstruct the attitude. This is the case, for example, for an IMU with only accelerometer and rate gyro sensors. Although the principal results of the chapter are developed in the matrix Lie group representation of $SO(3)$, the equivalent quaternion representation of the observers are also derived. The authors recommend that the quaternion representations are used for hardware implementation.

The body of the chapter consists of six sections. Section 2 provides a short discussion discussion on linear complementary filter design. Section 3 provides a quick overview of the sensor model, geometry of $SO(3)$ and introduces the notation used. Section 4 details the derivation of the direct and passive complementary passive filters. The development here is deliberately kept simple to be clear. Section 5 integrates on-line bias estimation into the observer design and provides a detailed stability analysis. Section 6 develops the *explicit complementary filter*, a reformulation of the passive complementary filter directly in terms of error measurements. A suite of experimental results, obtained during flight tests of the Hovereye (Fig. 7), are provided in Section 7 that demonstrate the performance of the proposed observers. Finally section 8 is devoted to concluding remarks.

2 A Review of complementary filtering

Complementary filters provide a means to fuse multiple independent noisy measurements of the same signal that have complementary spectral characteristics [1]. For example, consider two measurements $y_1 = x + \mu_1$ and $y_2 = x + \mu_2$ of a signal x where μ_1 is predominantly high frequency noise and μ_2 is a predominantly low frequency disturbance. Choosing a

pair of complementary transfer functions $F_1(s)+F_2(s)=1$ with $F_1(s)$ low pass and $F_2(s)$ high pass, the filtered estimate is given by

$$\hat{X}(s)=F_1(s)Y_1+F_2(s)Y_2=X(s)+F_1(s)\mu_1(s)+F_2(s)\mu_2(s).$$

The signal $X(s)$ is all pass in the filter output while noise components are high and low pass filtered as desired. This type of filter is also known as *distorsionless filtering* since the signal $x(t)$ is not distorted by the filter [5].

Complementary filters are particularly well suited to fusing low bandwidth position measurements with high band width rate measurements for first order kinematic systems. Consider the linear kinematics

$$\dot{x}=u. \tag{1}$$

with typical measurement characteristics

$$y_x=L(s)x+\mu_x,\quad y_u=u+\mu_u+b(t) \tag{2}$$

where $L(s)$ is low pass filter associated with sensor characteristics, μ represents noise in both measurements and $b(t)$ is a deterministic perturbation that is dominated by low-frequency content. Normally the low pass filter $L(s)\approx 1$ over the frequency range on which the measurement y_x is of interest. The rate measurement is integrated $\frac{y_u}{s}$ to obtain an estimate of the state and the noise and bias characteristics of the integrated signal are dominantly low frequency effects. Choosing

$$F_1(s)=\frac{C(s)}{C(s)+s}$$

$$F_2(s)=1-F_1(s)=\frac{s}{C(s)+s}$$

with $C(s)$ all pass such that $L(s)F_1(s)\approx 1$ over the bandwidth of $L(s)$. Then

$$\hat{X}(s)\approx X(s)+F_1(s)\mu_x(s)+\frac{\mu_u(s)+b(s)}{C(s)+s}$$

By suitable choice of $C(s)$ it is possible to tune the filters $F_1(s)$ and $1/(C(s)+s)$ to obtain satisfactory noise attenuation.

In practice, the filter structure is implemented by exploiting the complementary sensitivity structure of a linear feedback system subject to load disturbance. Consider the block diagram in Figure 1.

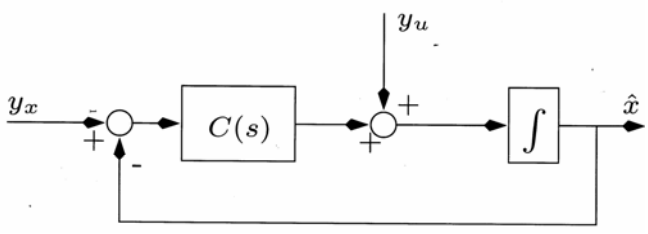

Fig. 1. Block diagram of a classical complementary filter

The output $\hat{x}$ can be written

$$\hat{x}(s) = \frac{C(s)}{s + C(s)} y_x(s) + \frac{s}{C(s) + s} \frac{y_u(s)}{s}$$

$$= T(s) y_x(s) + S(s) \frac{y_u(s)}{s}$$

where $S(s)$ is the sensitivity function of the closed-loop system and $T(s)$ is the complementary sensitivity. This architecture is easy to implement efficiently and allows one to use classical control design techniques for $C(s)$ in the filter design.

The simplest choice is a proportional feedback $C(s) = k_P$. In this case the closed-loop dynamics of the filter are given by

$$\dot{\hat{x}} = y_u + k_P (y_x - \hat{x}). \tag{3}$$

The frequency domain complementary filters associated with this choice are $F_1(s) = \frac{k_P}{s + k_P}$ and $F_2(s) = \frac{s}{s + k_P}$. Note that the crossover frequency for the filter is at k_P rad/s. The gain k_P is typically chosen based on the low pass characteristics of y_x and the low frequency noise characteristics of y_u to choose the best crossover frequency to tradeoff between the two measurements. If the rate measurement bias, $b(t) = b_0$, is a constant then it is natural to add an integrator into the compensator to make the system type I

$$C(s) = k_P + \frac{k_I}{s}. \tag{4}$$

A type I system will reject the constant load disturbance b_0 from the output. Gain design for k_P and k_I is typically based on classical frequency design methods.

The non-linear development in the body of the chapter requires a Lyapunov analysis of closed-loop system Eq. 3. Applying the PI compensator, Eq. 4, one obtains state space filter with dynamics

$$\dot{\hat{x}} = y_u - \hat{b} + k(y_x - \hat{x}), \quad \dot{\hat{b}} = -k_I(y_x - \hat{x})$$

The negative sign in the integrator state is introduced to indicate that the state $\hat{b}$ will cancel the bias in y_u. Consider the Lyapunov function

$$L = \frac{1}{2}|x - \hat{x}|^2 + \frac{1}{2k_I}|b_0 - \hat{b}|^2$$

Abusing notation for the noise processes, and using $\tilde{x} = (x - \hat{x})$, and $\tilde{b} = (b_0 - \hat{b})$, one has

$$\frac{d}{dt}L = -k_P|\tilde{x}|^2 - \mu_u\tilde{x} + \mu_x(\tilde{b} - k\tilde{x})$$

In the absence of noise one may apply Lyapunov's direct method to prove convergence of the state estimate. LaSalles principal of invariance may be used to show that $\hat{b} \to b_0$. When the underlying system is linear, then the linear form of the feedback and adaptation law ensure that the closed-loop system is linear and stability implies exponential stability. £

3 Notation and definitions.

3.1 Notation and mathematical identities

The special orthogonal group is denoted $SO(3)$. The associated Lie-algebra is the set of anti-symmetric matrices

$$so(3) = \{A \in R^{3\times 3} \mid A = -A^T\}$$

For any two matrices $A, B \in R^{n\times n}$ then the Lie-bracket (or matrix commutator) is $[A, B] = AB - BA$. Let $\Omega \in R^3$ then we define

$$\Omega_\times = \begin{pmatrix} 0 & -\Omega_3 & \Omega_2 \\ \Omega_3 & 0 & -\Omega_1 \\ -\Omega_2 & \Omega_1 & 0 \end{pmatrix}.$$

For any $v \in R^3$ then $\Omega_\times v = \Omega \times v$ is the vector cross product. The operator $\text{vex} : \mathsf{so}(3) \to R^3$ denotes the inverse of the $\Omega_\times$ operator

$$\text{vex}\left(\Omega_\times\right) = \Omega, \quad \Omega \in R^3.$$
$$\text{vex}(A)_\times = A, \quad A \in \mathsf{so}(3)$$

For any two matrices $A, B \in R^{n \times n}$ the Euclidean matrix inner product and Frobenius norm are defined

$$<< A, B >> = \text{tr}(A^T B) = \sum_{i,j=1}^{n} A_{ij} B_{ij}$$

$$||A|| = \sqrt{<< A, A >>} = \sqrt{\sum_{i,j=1}^{n} A_{ij}^2}$$

The following identities are used in the chapter

$$(Rv)_\times = R v_\times R^T, R \in SO(3), \quad v \in R^3$$
$$(v \times w)_\times = [v_\times, w_\times], \qquad v, w \in R^3$$
$$v^T w = < v, w > = \frac{1}{2} << v_\times, w_\times >>, \qquad v, w \in R^3$$
$$v^T v = |v|^2 = \frac{1}{2} ||v_\times||^2, \qquad v \in R^3$$
$$<< A, v_\times >> = 0, \qquad A = A^T \in R^3, \quad v \in R^3$$
$$\text{tr}([A, B]) = 0, \qquad A, B \in R^{3 \times 3}$$

The following notation for frames of reference is used

- $\{A\}$ denotes an inertial (fixed) frame of reference.
- $\{B\}$ denotes a body-fixed-frame of reference.
- $\{E\}$ denotes the estimator frame of reference.

Let P_a, P_s denote, respectively, the anti-symmetric and symmetric projection operators in square matrix space

$$P_a(H) = \frac{1}{2}(H - H^T), \qquad P_s(H) = \frac{1}{2}(H + H^T).$$

Let (θ, a) $(|a|=1)$ denote the angle-axis coordinates of $R \in SO(3)$. One has

$$R = \exp(\theta a_\times), \qquad \log(R) = \theta a_\times$$

$$\cos(\theta) = \frac{1}{2}(\mathrm{tr}(R) - 1), \qquad P_a(R) = \sin(\theta) a_\times.$$

For any $R \in SO(3)$ then $3 \geq \mathrm{tr}(R) \geq -1$. If $\mathrm{tr}(R) = 3$ then $\theta = 0$ in angle-axis coordinates and $R = I$. If $\mathrm{tr}(R) = -1$ then $\theta = \pm\pi$, R has real eigenvalues $(1, -1, -1)$.

The unit quaternion representation of rotations is commonly used for the realisation of algorithms on $SO(3)$ since it offers considerable efficiency in code implementation. The set of quaternions is denoted $Q = \{q = (s, v) \in R \times R^3 : |q| = 1\}$. The set Q is a group under the operation

$$q_1 \otimes q_2 = \begin{bmatrix} s_1 s_2 - v_1^T v_2 \\ s_1 v_2 + s_2 v_1 + v_1 \times v_2 \end{bmatrix}$$

with identity element $1 = (1, 0, 0, 0)$. The group of quaternions are homomorphic to $SO(3)$ via the map

$$F : Q \to SO(3), \quad F(q) := I_3 + 2sv_\times + 2v_\times^2$$

This map is a two to one mapping of Q onto $SO(3)$ with kernel $\{(1, 0, 0, 0), (-1, 0, 0, 0)\}$, thus, Q is locally isomorphic to $SO(3)$ via F. Given $R \in SO(3)$ such that $R = \exp(\theta a_\times)$ then $F^{-1}(R) = \{\pm(\cos(\frac{\theta}{2}), \sin(\frac{\theta}{2})a)\}$. Let $\Omega \in \{A\}$ denote a body-fixed frame velocity, then the pure quaternion $\mathbf{p}(\Omega) = (0, \Omega)$ is associated with a quaternion velocity.

3.2 Measurements

The measurements available from a typical inertial measurement unit are 3-axis rate gyros, 3-axis accelerometers and 3-axis magnetometers measurements. The reference frame of the strap down IMU is termed the body-fixed-frame $\{B\}$. The inertial frame is denoted $\{A\}$. The rotation $R = R_B^A$ denotes the relative orientation of $\{B\}$ with respect to $\{A\}$.

Rate Gyros: The rate gyro measures angular velocity of $\{B\}$ relative to $\{A\}$ expressed in the body-fixed-frame of reference $\{B\}$. The error model used is

$$\Omega^y = \Omega + b + \mu \in R^3$$

where $\Omega \in \{B\}$ denotes the true value, μ denotes additive measurement noise and b denotes a constant (or slowly time-varying) gyro bias.

Accelerometer: Denote the instantaneous linear acceleration of $\{B\}$ relative to $\{A\}$, expressed in $\{A\}$, by $\dot{v}$. An ideal accelerometer, 'strapped down' to the body-fixed-frame $\{B\}$, measures the instantaneous linear acceleration of $\{B\}$ minus the (conservative) gravitational acceleration field g_0 (where we consider g_0 expressed in the inertial frame $\{A\}$), and provides a measurement expressed in the body-fixed-frame $\{B\}$. In practice, the output a from a MEMS component accelerometer has added bias and noise,

$$a = R^T(\dot{v} - g_0) + b_a + \mu_a,$$

where b_a is a bias term and μ_a denotes additive measurement noise. Normally, the gravitational field $g_0 = |g_0| e_3$ where $|g_0| \approx 9.8$ dominates the value of a for low frequency response. Thus, it is common to use

$$v_a = \frac{a}{|a|} \approx -R^T e_3$$

as a low-frequency estimate of the inertial z-axis expressed in the body-fixed-frame.

Magnetometer: The magnetometers provide measurements of the magnetic field

$$m = R^T m^A + B_m + \mu_b$$

where m^A is the Earths magnetic field (expressed in the inertial frame), B_m is a body-fixed-frame expression for the local magnetic disturbance and μ_b denotes measurement noise. The noise μ_b is usually quite low for magnetometer readings, however, the local magnetic disturbance can be very significant, especially if the IMU is strapped down to a mAV with electric motors. Only the direction of the magnetometer output is relevant for attitude estimation and we will use a vectorial measurement

$$v_m = \frac{m}{|m|}$$

in the following development

The measured vectors v_a and v_m can be used to construct an instantaneous algebraic measurement of the rotation $R_B^A : \{B\} \to \{A\}$

$$R_y = \arg \min_{R \in SO(3)} \left(\lambda_1 \mid e_3 - Rv_a \mid^2 + \lambda_2 \mid v_m^A - Rv_m \mid^2 \right) \approx R_A^B$$

where v_m^A is the inertial direction of the magnetic field in the locality where data is acquired. The weights λ_1 and λ_2 are chosen depending on the relative confidence in the sensor outputs. Due to the computational complexity of solving an optimisation problem the reconstructed rotation is often obtained in a suboptimal manner where the constraints are applied in sequence; that is, two degrees of freedom in the rotation matrix are resolved by the acceleration readings and the final degree of freedom is resolved using the magnetometer. As a consequence, the error properties of the reconstructed attitude R_y can be difficult to characterise.

Moreover, if either magnetometer or accelerometer readings are unavailable (due to local magnetic disturbance or high acceleration manoeuvres) then it is impossible to resolve the vectorial measurements into a unique instantaneous algebraic measurement of attitude.

3.3 Error criteria for estimation on $SO(3)$

Let $\hat{R}$ denote an estimate of the body-fixed rotation matrix $R = R_B^A$. The rotation $\hat{R}$ can be considered as coordinates for the estimator frame of reference $\{E\}$. It is also associated with the frame transformation

$$\hat{R} = \hat{R}_E^A : \{E\} \to \{A\}.$$

The goal of attitude estimate is to drive $\hat{R} \to R$. The estimation error we propose to use is the relative rotation from body-fixed-frame $\{B\}$ to the estimator frame $\{E\}$

$$\tilde{R} := \hat{R}^T R, \qquad \tilde{R} = \tilde{R}_B^E : \{B\} \to \{E\}. \tag{5}$$

The proposed observer design is based on Lyapunov stability analysis. The Lyapunov functions used are inspired by the cost function

$$E_{tr} := \frac{1}{2} \| I_3 - \tilde{R} \|^2 = \frac{1}{2} \mathrm{tr}(I_3 - \tilde{R}) \tag{6}$$

One has that

$$E_{tr} := \frac{1}{2}\mathrm{tr}(I - \tilde{R}) = (1 - \cos(\theta)) = 2\sin(\theta/2)^2. \quad (7)$$

where θ is the angle associated with the rotation from $\{B\}$ to frame $\{E\}$. Thus, driving Eq. 6 to zero ensures that $\theta \to 0$.

4 Complementary filters on $SO(3)$

In this section, a general framework for non-linear complementary filtering on the special orthogonal group is introduced. The theory is first developed for the idealised case where $R(t)$ and $\Omega(t)$ are assumed to be known and used to drive the filter dynamics. Filter design for real world signals is considered in later sections.

The goal of attitude estimation is to provide a set of dynamics for an estimate $\hat{R}(t) \in SO(3)$ to drive the error rotation (Eq. 5) $\tilde{R}(t) \to I_3$. The kinematics of the true system are

$$\dot{R} = R\Omega_\times = (R\Omega)_\times R \quad (8)$$

where $\Omega \in \{B\}$. The proposed observer equation is posed directly as a kinematic system for an attitude estimate $\hat{R}$ on $SO(3)$. The observer kinematics include a prediction term based on the Ω measurement and an innovation or correction term, $k_P\omega$, with $\omega := \omega(\tilde{R})$ derived from the error $\tilde{R}$ and $k_P > 0$ a positive gain. The general form proposed for the observer is

$$\dot{\hat{R}} = (R\Omega + k_P\hat{R}\omega)_\times \hat{R}, \qquad \hat{R}(0) = \hat{R}_0. \quad (9)$$

The term $(R\Omega + k_P\hat{R}\omega) \in \{A\}$ is expressed in the inertial frame. The body-fixed-frame angular velocity is mapped back into the inertial frame $\Omega^A = R\Omega$. If no correction term is used ($k_P\omega \equiv 0$) then the error rotation $\tilde{R}$ is constant,

$$\dot{\tilde{R}} = \hat{R}^T(R\Omega)_\times^T R + \hat{R}^T(R\Omega)_\times R = \hat{R}^T\left(-(R\Omega)_\times + (R\Omega)_\times\right)R = 0. \quad (10)$$

The correction term $k_p\omega$ consists of a proportional gain $k_P > 0$ and the vector error term $\omega := \omega(\tilde{R}) \in \{E\}$, considered to be in the estimator frame of reference. The vector error term can be thought of as a non-linear approximation of the error between R and $\hat{R}$. In practice, it will be implemented as an error between a measured estimate R_y of R and the estimate $\hat{R}$. The goal of the observer design is to find a simple expression for ω that leads to robust convergence of $\tilde{R} \to I$. In this chapter we consider the choice

$$\omega = \text{vex}(P_a(\tilde{R})). \tag{11}$$

Lemma 1. [Complementary filter.] Consider the attitude kinematics (Eq. 8) and assume that R and Ω are known. Choose ω according to Eq. 11 and choose $k_P > 0$ a positive gain. Let $\hat{R}(t)$ denote the solution of Eq. 9 for initial condition $\hat{R}_0$. Then

$$\dot{E}_{tr} = -2k_P \cos^2(\theta/2) E_{tr}$$

where E_{tr} is defined in Eq. 7. For any initial condition $\hat{R}_0$ such that $\text{tr}(\tilde{R}_0) \neq -1$ then $\hat{R}(t) \to R(t)$ exponentially.

Proof: Deriving the Lyapunov function E_{tr} subject to dynamics Eq. 9 yields

$$\begin{aligned}
\dot{E}_{tr} &= -\frac{1}{2}\text{tr}(\dot{\tilde{R}}) = -\frac{k_P}{2}\text{tr}\left(\omega_\times^T \tilde{R}\right) \\
&= -\frac{k_P}{2}\text{tr}\left[\omega_\times^T (P_s(\tilde{R}) + P_a(\tilde{R}))\right] = -\frac{k_P}{2}\text{tr}\left[\omega_\times^T P_a(\tilde{R})\right] \\
&= -\frac{k_P}{2} << \omega_\times, P_a(\tilde{R}) >>
\end{aligned}$$

Substituting for ω, Eq. 11, yields

$$E_{tr} = -\frac{k_P}{2} || P_a(\tilde{R}) ||^2 = -k_P | \omega |^2 .$$

Defining θ by the angle axis convention $\sin(\theta) a_\times = P_a(\tilde{R})$ for $|a| = 1$, one has $|| a_\times || = 2$ and

$$\begin{aligned}
E_{tr} &= -k_P \sin^2(\theta) || a_\times ||_\times^2 = -2k_P \sin^2(\theta) \\
&= -8k_P \sin^2(\theta/2)\cos^2(\theta/2) = -2k_P \cos^2(\theta/2) E_{tr}.
\end{aligned}$$

The condition on the initial condition $\tilde{R}_0$ guarantees that $-\pi < \theta_0 < \pi$. The result follows from applying Lyapunov's direct method. QED.

We term the filter Eq. 9 a *complementary filter on* $SO(3)$ since it recaptures the block diagram structure of a classical complementary filter (cf. §2).

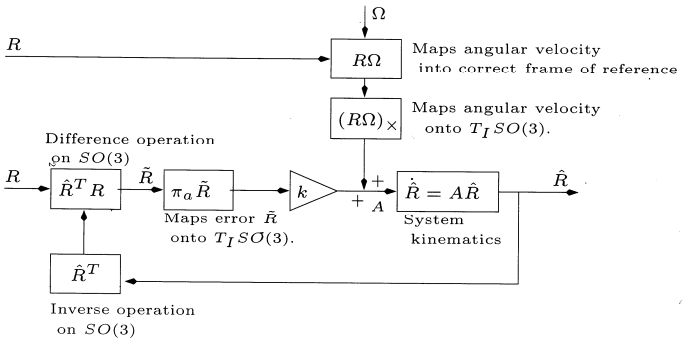

Fig. 2. Block diagram of the general form of a complementary filter on $SO(3)$

In Figure 2: The '$\hat{R}^T$' operation is an inverse operation on $SO(3)$ and is equivalent to a '$-$' operation for a linear complementary filter. The '$\hat{R}^T R$' operation is equivalent to generating the error term '$y - \hat{x}$'. The two operations $P_a(\tilde{R})$ and $(R\Omega)_\times$ are maps from error space and velocity space into the tangent space of $SO(3)$; operations that are unnecessary on Euclidean space due to the identification $T_x R^n \equiv R^n$. The kinematic model is the Lie-group equivalent of a first order integrator.

To implement the complementary filter it is necessary to map the body-fixed-frame velocity Ω into the inertial frame. In practice, the 'true' rotation R is not available and an estimate of the rotation must be used. Two possibilities are considered:

direct complementary filter: The constructed attitude R_y is used to map the velocity into the inertial frame $\Omega^A \approx R_y \Omega_y$. A block diagram of this filter design is shown in Figure 3. This approach can be linked to observers documented in earlier work [29,32]. The ap-

proach has the advantage that it does not introduce an additional feedback loop in the filter dynamics, however, noise in the reconstructed attitude R_y will enter into the feed-forward term of the filter.

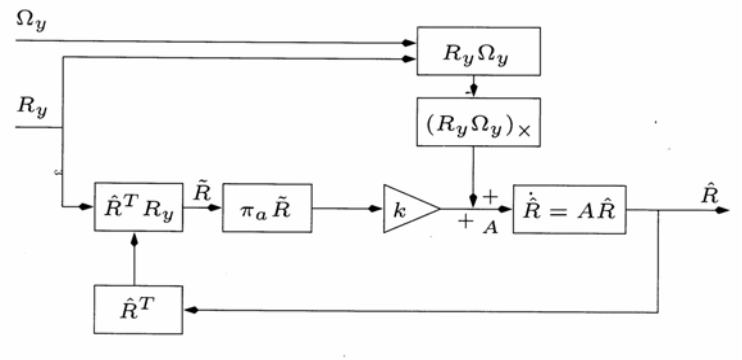

Fig. 3. Block diagram of the direct complementary filter on $SO(3)$

passive complementary filter: The filtered attitude $\hat{R}$ is used in the predictive velocity term $\Omega^A \approx \hat{R}\Omega_y$. A block diagram of this architecture is shown in Figure 4. The advantage lies in avoiding corrupting the predictive angular velocity term with the noise in the reconstructed pose. However, the approach introduces a secondary feedback loop in the filter and stability needs to be proved.

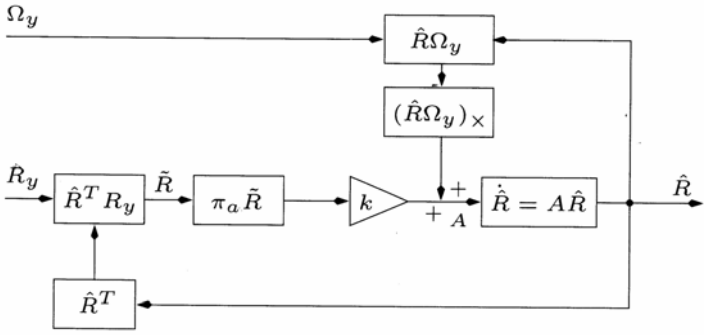

Fig. 4. Block diagram of the passive complementary filter on $SO(3)$

Lemma 2. [Passive complementary filter.] Consider the rotation kinematics Eq. 8 and assume that R and Ω are known. Let $k_P > 0$

and choose ω according to Eq. 11. Let the attitude estimate $\hat{R}(t)$ be given by the solution of

$$\dot{\hat{R}} = \left(\hat{R}\Omega + k_P \hat{R}\omega\right)_\times \hat{R}, \qquad \hat{R}(0) = \hat{R}_0 \tag{12}$$

Then

$$\dot{E}_{tr} = -2k_P \cos^2(\theta/2) E_{tr}$$

where E_{tr} is defined in Eq. 7. For any initial condition $\hat{R}_0$ such that $\mathrm{tr}(\tilde{R}_0) \neq -1$, then $\hat{R}(t) \to R(t)$ exponentially.

Proof: Observe that

$$\left(\hat{R}\Omega + k_P \hat{R}\omega\right)_\times \hat{R} = \hat{R}\left(\Omega + k_P \omega\right)_\times \hat{R}^T \hat{R} = \hat{R}\left(\Omega + k_P \omega\right)_\times$$

Differentiating E_{tr} subject to dynamics Eq. 12 yields

$$\begin{aligned} E_{tr} &= -\frac{1}{2}\mathrm{tr}(\dot{\tilde{R}}) = -\frac{1}{2}\mathrm{tr}(-(\Omega + k_P\omega)_\times \tilde{R} + \tilde{R}\Omega_\times) \\ &= -\frac{1}{2}\mathrm{tr}([\tilde{R}, \Omega_\times]) - \frac{k_P}{2}\mathrm{tr}(\omega_\times^T \tilde{R}) \\ &= -\frac{k_P}{2} << \omega_\times, P_a(\tilde{R}) >> \end{aligned}$$

since the trace of a commutator is zero, $\mathrm{tr}([\tilde{R}, \Omega_\times]) = 0$, a property of the passivity of the rotational kinematics on $SO(3)$. The remainder of the proof is identical to that of Lemma 1. QED.

It is important to note that the direct and the passive complementary filters have different solutions even though the Lyapunov stability analysis appears identical. The different trajectories of $\hat{R}e_3$ are shown in Figure 5 for identical initial conditions and constant angular velocity Ω. The level sets of the Lyapunov function are the small circles of the hemisphere and the two trajectories always lie on the same small circle during the evolution of the filter.

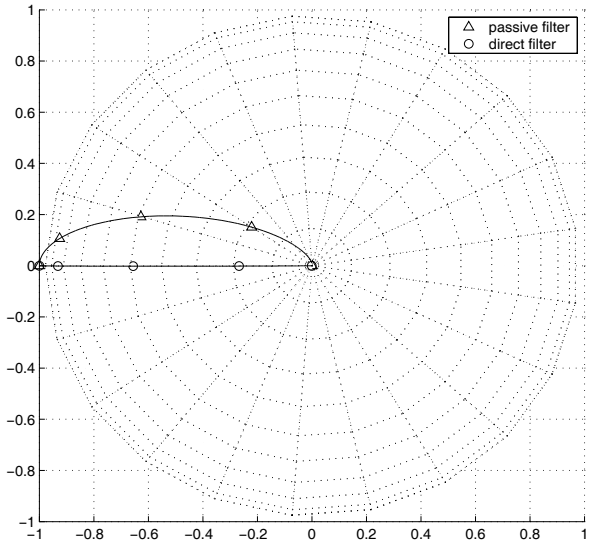

Fig. 5. Trajectories of $\tilde{R}e_3$ for direct and passive complementary filters on the plan $\{e_1, e_2\}$ for initial deviation, $\tilde{R}_0$, corresponding to a rotation of $\frac{\pi}{2}$ rad around the e_2 axis and $\Omega = 0.3e_3$ rad/s

If $\mathrm{tr}(\tilde{R})(0) = -1$, then for both the direct and passive filter, it is easily verified that $\mathrm{tr}(\dot{R}(t)) = 0$ for all $t \geq 0$. Hence, the set $U_0 = \{\tilde{R} \in SO(3) : \mathrm{tr}(\tilde{R}) = -1\}$ is an invariant set of the error dynamics. This set corresponds to a maximum of the cost function E_{tr} and the descent condition in the Lyapunov arguments for both filters ensures that the invariant set is unstable.

There is no particular theoretical advantage to either the direct or the passive filter architecture in the case where exact measurements are assumed. However, it is straightforward to see that the passive filter (Eq. 12) can be written

$$\dot{\hat{R}} = \hat{R}(\Omega_\times + k_P P_a(\tilde{R})). \tag{13}$$

This formulation suppresses entirely the requirement to represent Ω and $\omega = k_P P_a(\tilde{R})$ in the inertial frame and leads to the architecture shown in Figure 6. The passive complementary filter avoids coupling the reconstructed attitude noise into the predictive velocity term of the observer, has a strong Lyapunov stability analysis

(Lemma 2), and provides a simple and elegant realisation that will lead to the results in Section 6.

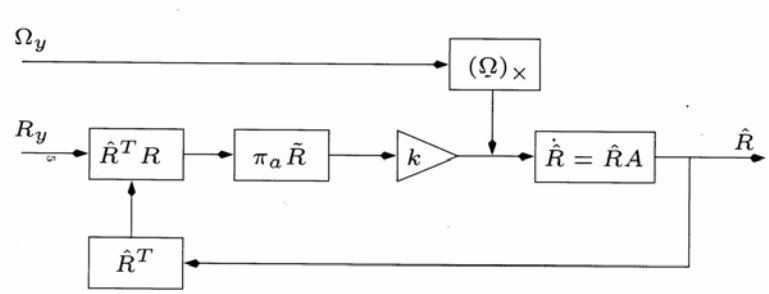

Fig. 6. Block diagram of the simplified form of the passive complementary filter

5. Adaptive gyro bias compensation

In this section, the direct and passive complementary filters on $SO(3)$ are extended to provide on-line estimation of time-varying bias terms in the gyroscope measurements.

For the following work it is assumed that a reconstructed rotation R_y and a biased measure of angular velocity Ω^y are available

$$R_y \approx R, \qquad \text{valid for low frequencies,} \tag{14}$$

$$\Omega_y \approx \Omega + b, \qquad \text{for constant bias } b. \tag{15}$$

The approach taken is to add an integrator to the compensator term in the feedback equation of the complementary filter.

Let $k_P, k_I > 0$ be positive gains and define:

Direct complementary filter with bias correction:

$$\dot{\hat{R}} = \left(R_y(\Omega^y - \hat{b}) + k_P \hat{R}\omega \right)_\times \hat{R}, \quad \hat{R}(0) = \hat{R}_0, \tag{16}$$

$$\dot{\hat{b}} = -k_I \omega, \quad \hat{b}(0) = \hat{b}_0, \tag{17}$$

$$\omega = \text{vex}(P_a(\tilde{R})), \quad \tilde{R} = \hat{R}^T R_y. \tag{18}$$

Passive complementary filter with bias correction:

$$\dot{\hat{R}} = \hat{R}\left(\Omega^{y} - \hat{b} + k_P\omega\right)_{\times}, \quad \hat{R}(0) = \hat{R}_0, \tag{19}$$

$$\dot{\hat{b}} = -k_I\omega, \quad \hat{b}(0) = \hat{b}_0, \tag{20}$$

$$\omega = \mathrm{vex}(P_a(\tilde{R})), \quad \tilde{R} = \hat{R}^T R_y. \tag{21}$$

The additional dynamics introduced for the $\hat{b}$ term can be thought of as an adaptive estimate of the gyro bias. The stability analysis is based on the same approach as the adaptive control Lyapunov function interpretation of the classical complementary filter presented in Section 2. The non-linear state space $SO(3)$ introduces several complexities to the analysis, the most important following from the existence of local maxima of the Lyapunov function due to the topological structure of $SO(3)$. The proofs of the following two theorems are contained in the technical report [18]. Local stability results are given in [19].

Theorem 1. [Direct complementary filter with bias correction] Consider the rotation kinematics Eq. 8 for a time-varying $R(t) \in SO(3)$ and with measurements given by Eq. 14-15. Let $(\hat{R}(t), \hat{b}(t))$ denote the solution of Eq. 16-18. Define error variables $\tilde{R} = \hat{R}^T R$ and $\tilde{b} = b - \hat{b}$. Define $U \subseteq SO(3) \times R^3$ by

$$U = \left\{(\tilde{R}, \tilde{b}) \mid \mathrm{tr}(\tilde{R}) = -1, P_a(\tilde{b}_{\times}\tilde{R}) = 0\right\}. \tag{22}$$

Then:

1. The set U is forward invariant and unstable with respect to the dynamic system Eq. 16-18.
2. The error $(\tilde{R}(t), \tilde{b}(t))$ is locally exponentially stable to $(I, 0)$.
3. For almost all initial conditions $(\tilde{R}_0, \tilde{b}_0) \notin U$ the trajectory $(\hat{R}(t), \hat{b}(t))$ converges to the trajectory $(R(t), b)$.

Theorem 2. [Passive complementary filter with bias correction] Consider the rotation kinematics Eq. 8 for a time-varying $R(t) \in SO(3)$ and with measurements given by Eq. 14-15. Let $(\hat{R}(t), \hat{b}(t))$ denote the solution of Eq. 19-21. Define error variables

$\tilde{R} = \hat{R}^T R$ and $\tilde{b} = b - \hat{b}$ and assume that $\Omega(t)$ is a bounded, absolutely continuous signal that is persistently exciting and uncorrelated to the error signal $\tilde{R} = \hat{R}^T R$. Define $U_0 \subseteq SO(3) \times R^3$ by

$$U_0 = \left\{ (\tilde{R}, \tilde{b}) \mid \mathrm{tr}(\tilde{R}) = -1, \tilde{b} = 0 \right\}. \tag{23}$$

Then:

1. The set U_0 is forward invariant and unstable with respect to the dynamic system 19-21.
2. The error $(\tilde{R}(t), \tilde{b}(t))$ is locally exponentially stable to $(I, 0)$.
3. For almost all initial conditions $(\tilde{R}_0, \tilde{b}_0) \notin U_0$ the trajectory $(\hat{R}(t), \hat{b}(t))$ converges to the trajectory $(R(t), b)$.

Apart from the expected conditions inherited from Theorem 1 the key assumption in Theorem 2 is the persistence of excitation of $\Omega(t)$. The perturbation of the passive dynamics by the driving term Ω provides a disturbance that ensures that the adaptive bias estimate converges to the true gyroscopes' bias, a particularly useful property in practical applications.

4.1 Quaternion versions of direct and passive complementary filters

Consider the rotation kinematics on $SO(3)$ Eq. 8. The associated quaternion kinematics are given by

$$\dot{q} = \frac{1}{2} q \otimes \mathbf{p}(\Omega) \tag{24}$$

Let $q_y \approx q$ be a low frequency measure of q, and $\Omega_y \approx \Omega + b$ (for constant bias b) be the angular velocity measure. Let $\hat{q}$ denote the observer estimate and quaternion error $\tilde{q}$

$$\tilde{q} = \hat{q}^{-1} \otimes q = \begin{bmatrix} \tilde{s} \\ \tilde{v} \end{bmatrix}$$

Note that

$$2\tilde{s}\tilde{v} = 2\cos(\theta/2)\sin(\theta/2)a = \frac{1}{2}(\sin\theta)a = \text{vex}(P_a(\tilde{R}))$$

where (θ, a) is the angle axis representation of $\tilde{R} = F(\tilde{q})$.

The direct complimentary filter is closely related to quaternion based attitude filters published over the last fifteen years [29,34,32]. The quaternion representation of the *Direct complementary filter (Eq. 16-18)* is:

$$\dot{\hat{q}} = \frac{1}{2}\hat{q} \otimes \mathbf{p}(\tilde{R}(\Omega_y - \hat{b}) + 2k_P\tilde{s}\tilde{v}) \quad (25)$$

$$\dot{\hat{b}} = -2k_I\tilde{s}\tilde{v} \quad (26)$$

There is a fifteen year history of using the quaternion representation and Lyapunov design methodology for filtering on $SO(3)$ (for example cf. [34,29,32]). To the authors knowledge the Lyapunov analysis in all cases has been based around the cost function

$$\Phi(\tilde{q}) = (|\tilde{s}| - 1)^2 + |\tilde{v}|^2 .$$

Due to the unit norm condition it is straightforward to show that

$$\Phi(\tilde{q}) = 2(1 - |\tilde{s}|) = 2\left(1 - |\cos(\theta/2)|\right)$$

The cost function proposed in this chapter is $E_{tr} = (1 - \cos(\theta))$ (Eq. 7). It follows that the quadratic approximation of both cost functions around the point $\theta = 0$ is the quadratic $\theta^2/2$. The quaternion cost function Φ, however, is non-differentiable at the point $\theta = \pm\pi$ while the cost $\text{tr}(I - \tilde{R})$ has a smooth local minima at this point.

Almost all quaternion filters in the published literature have a similar flavour that dates back to the seminal work of Salcudean [29]. The closest published work to that undertaken in the present chapter was published by Thienel in her doctoral dissertation [33] and paper [32]. The filter considered by Thienel *et al.[0.001mm]* is given by

$$\dot{\hat{q}} = \frac{1}{2}\hat{q} \otimes \mathbf{p}(\tilde{R}(\Omega_y - \hat{b} + k_P\text{sgn}(\tilde{s})\tilde{v})) \quad (27)$$

$$\dot{\hat{b}} = -k_I\text{sgn}(\tilde{s})\tilde{v} \quad (28)$$

The $\text{sgn}(\tilde{s})$ term enters naturally in the filter design from the differential, $\frac{d}{dt}|\tilde{s}| = \text{sgn}(\tilde{s})\frac{d}{dt}\tilde{s}$, of the absolute value term in the cost func-

tion Φ, during the Lyapunov design process.

Consider the observer obtained by replacing $\text{sgn}(\tilde{s})$ in Eqn's 27-28 by $2\tilde{s}$. Note that with this substitution, Eq. 28 is transformed into Eq. 26. To show that Eq. 27 transforms to Eq. 25 it is sufficient to show that $\tilde{R}\tilde{v} = \tilde{v}$. This is straightforward from

$$2\tilde{s}\tilde{R}\tilde{v} = \tilde{R}(2\tilde{s}\tilde{v}) = \tilde{R}\text{vex}(P_a(\tilde{R}))$$

$$= \text{vex}(\tilde{R}P_a(\tilde{R})\tilde{R}^T) = \text{vex}(P_a(\tilde{R})) = 2\tilde{s}\tilde{v}$$

It is shown that the quaternion filter Eqn's 27-28 is obtained from the standard form of the complimentary filter proposed Eq. 16-18 with the innovation term Eq. 18 replaced by

$$\omega_q = \text{sgn}(\tilde{s})\tilde{v}, \quad \tilde{q} \in F^{-1}(\hat{R}^T R).$$

Note that the innovation defined in Eq. 18 can be written $\omega = 2\tilde{s}\tilde{v}$. It follows that

$$\omega_q = \frac{\text{sgn}(\tilde{s})}{2\tilde{s}}\omega$$

The innovation term for the two filters varies only by the positive scaling factor $\text{sgn}(\tilde{s})/(2\tilde{s})$. The quaternion innovation ω_q is not well defined for $\tilde{s} = 0$ (where $\theta = \pm\pi$) and these points are not well defined in the filter dynamics 27-28. It should be noted, however, that $|\omega_q|$ is bounded at $\tilde{s} = 0$ and, apart from possible switching behaviour, the filter can still be implemented on the remainder of $SO(3) \times R^3$. An argument for the use of the innovation ω_q is that the resulting error dynamics strongly force the estimate away from the unstable set U (cf. Eq. 22). An argument against its use is that, in practice, such situations will only occur due to extreme transients that would overwhelm the bounded innovation term ω_q in any case, and cause the numerical implementation of the filter to deal with a discontinuous argument. In practice, it is an issue of little significance since the filter will work sufficiently well to avoid any issues with the set U for either choice of innovation. For $\tilde{s} \to 1$, corresponding to $\theta = 0$, the innovation ω_q scales to a factor of $1/2$ the innovation ω. A simple scaling factor like this is compensated for the in choice of filter gains k_P and k_I and makes no difference to

the performance of the filter.
The quaternion representation of the *Passive complementary filter (Eq. 19-21)* is:

$$\dot{\hat{q}} = \frac{1}{2}\hat{q} \otimes \mathbf{p}(\Omega_y - \hat{b} + 2k_P \tilde{s}\tilde{v}) \tag{29}$$

$$\dot{\hat{b}} = -2k_I \tilde{s}\tilde{v} \tag{30}$$

To the authors knowledge this version of the complementary filter on the quaternion group has not been considered in prior work. It is not surprising that the passive complementary filter has not been proposed by authors working purely in the quaternion representation since the passivity property is somewhat obscure in this representation.

6 Explicit error formulation of the passive complementary filter

A weakness of the implementation of both the direct and passive complementary filters is the requirement for a reconstructed estimate of the attitude, R_y, to use as the driving term for the error dynamics. The reconstruction cannot be avoided in the direct filter implementation because the reconstructed attitude is also used to transform the measured angular velocity into the inertial frame. In this section, we show how the passive complementary filter may be reformulated in terms of direct measurements from the inertial unit.
Let $v_{0i} \in \{A\}$, $i = 1,\ldots,n$, denote a set of n known inertial directions. The measurements considered are body-fixed-frame observations of the fixed inertial directions

$$v_i = R^T v_{0i} + \mu_i, \quad v_i \in \{B\} \tag{31}$$

where μ_i is a noise process. Since only the direction of the measurement is relevant to the observer we assume that $|v_{0i}| = 1$ and normalise all measurements to ensure $|v_i| = 1$.
Let $\hat{R}$ be an estimate of R. Define

$$\hat{v}_i = \hat{R}^T v_{0i}$$

to be the associated estimate of v_i. For a single direction v_i, the error considered is

$$E_i = 1 - \cos(\angle v_i, \hat{v}_i) = 1 - < v_i, \hat{v}_i >$$

which yields

$$E_i = 1 - \mathrm{tr}(\hat{R}^T v_{0i} v_{0i}^T R) = 1 - \mathrm{tr}(\tilde{R} R^T v_{0i} v_{0i}^T R)$$

For multiple measures v_i the following cost function is considered

$$E_{mes} = \sum_{i=1}^{n} k_i E_i = \sum_{i=1}^{n} k_i - \mathrm{tr}(\tilde{R} M), \quad k_i > 0, \tag{32}$$

where

$$M = R^T M_0 R \quad \text{with} \quad M_0 = \sum_{i=1}^{n} k_i v_{0i} v_{0i}^T \tag{33}$$

Assume linearly independent inertial direction $\{v_{0i}\}$ then the matrix M is positive definite $(M > 0)$ if $n \geq 3$. For $n \leq 2$ then M is positive semi-definite with one eigenvalue zero. The weights $k_i > 0$ are chosen depending on the relative confidence in the measurements v_i. For technical reasons in the proof of Theorem 1 we assume additionally that the weights k_i are chosen such that M_0 has three distinct eigenvalues $\lambda_1 > \lambda_2 > \lambda_3$.

A full proof of the following theorem is contained in the technical report [18]. A local stability proof is contained in the paper [11].

Theorem 1. [Explicit complementary filter with bias correction] Consider the rotation kinematics Eq. 8 for a time-varying $R(t) \in SO(3)$ and with measurements given by Eqn's 31 and 15. Assume that there are two or more, ($n \geq 2$) vectorial measurements v_i available. Choose $k_i > 0$ such that M_0 (defined by Eq. 33) has three distinct eigenvalues. Consider the filter kinematics given by

$$\dot{\hat{R}} = \hat{R}\left((\Omega^y - \hat{b})_\times + k_P (\omega_{mes})_\times \right), \quad \hat{R}(0) = \hat{R}_0 \tag{34}$$

$$\dot{\hat{b}} = -k_I \omega_{mes} \tag{35}$$

$$\omega_{mes} := \sum_{i=1}^{n} k_i v_i \times \hat{v}_i, \qquad k_i > 0. \tag{36}$$

and let $(\hat{R}(t), \hat{b}(t))$ denote the solution of Eqn's 34-36. Assume that $\Omega(t)$ is a bounded, absolutely continuous signal that is persistently exciting and uncorrelated to the error signal $\tilde{R} = \hat{R}^T R$. Then:

1. There are three unstable equilibria of the filter characterised by

$$(\hat{R}_{*i}, \hat{b}_{*i}) = \left(U_0 D_i U_0^T R, b\right), i = 1, 2, 3,$$

2. where $D_1 = \text{diag}(1,-1,-1)$, $D_2 = \text{diag}(-1,1,-1)$ and $D_3 = \text{diag}(1,-1,-1)$ are diagonal matrices with entries as shown and $U_0 \in SO(3)$ such that $M_0 = U_0 \Lambda U_0^T$ where $\Lambda = \text{diag}(\lambda_1, \lambda_2, \lambda_3)$ is a diagonal matrix.
3. The error $(\tilde{R}(t), \tilde{b}(t))$ is locally exponentially stable to $(I, 0)$.
4. For almost all initial conditions $(\tilde{R}_0, \tilde{b}_0) \neq (\hat{R}_{*i}^T R, b)$, $i = 1, \ldots, 3$, the trajectory $(\hat{R}(t), \hat{b}(t))$ converges to the trajectory $(R(t), b)$.

The quaternion representation of *Explicit complementary filter (Eq. 34-36)* is:

$$\omega_{mes} = -\text{vex}\left(\sum_{i=1}^{n} \frac{k_i}{2} (v_i v_i^T - \hat{v}_i v_i^T)\right) \ldots \qquad (37)$$

$$\dot{\hat{q}} = \frac{1}{2} \hat{q} \otimes \mathbf{p}(\Omega_y - \hat{b} + k_P \omega_{mes}) \qquad (38)$$

$$\dot{\hat{b}} = -k_I \omega_{mes} \ldots\ldots\ldots\ldots\ldots\ldots\ldots.. \qquad (39)$$

If $n = 3$, the weights $k_i = 1$, and the measured directions are orthogonal $(v_i^T v_j = 0, \forall i \neq j)$ then $M = I_3$. The cost function E_{mes} becomes

$$E_{mes} = 3 - \text{tr}(\tilde{R} M) = \text{tr}(I_3 - \tilde{R}) = E_{tr}.$$

In this case, the explicit complementary filter (Eqn's 34-36) and the passive complementary filter (Eqn's 19-21) are identical.

If $n = 2$, the two typical measurements obtained from an IMU unit are estimates of the gravitational, a, and magnetic, m, vector fields

$$v_a = R^T \frac{a_0}{|a_0|}, \qquad v_m = R^T \frac{m_0}{|m_0|}.$$

The cost function E_{mes} becomes

$$E_{mes} = k_1(1 - < \hat{v}_a, v_a >) + k_2(1 - < \hat{v}_m, v_m >)$$

The weights k_1 and k_2 are introduced to weight the confidence in each measure. In situations where the IMU is subject to high magnitude accelerations (such as during takeoff or landing manoeuvres) it may be wise to reduce the relative weighting of the accelerometer data ($k_1 << k_2$) compared to the magnetometer data. Conversely, in many applications the IMU is mounted in the proximity to powerful electric motors and their power supply busses leading to low confidence in the magnetometer readings (choose $k_1 >> k_2$). This is a very common situation in the case of mini aerial vehicles with electric motors. In extreme cases the magnetometer data is unusable and provides motivation for a filter based solely on accelerometer data.

1. Estimation from the measurements of a single direction

Let v_a be a measured body fixed frame direction associated with a single inertial direction v_{0a}, $v_a = R^T v_{0a}$. Let $\hat{v}_a$ be an estimate $\hat{v}_a = \hat{R}^T v_{0a}$. The error considered is

$$E_{mes} = 1 - \mathrm{tr}(\tilde{R}M); \quad M = R^T v_{0a} v_{0a}^T R$$

A proof to the following corollary is provided in the technical report [18]. Local stability is proved in the paper [11].

Corollary 2. Consider the rotation kinematics Eq. 8 for a time-varying $R(t) \in SO(3)$ and with measurements given by Eqn's 31 (for a single measurement $v_1 = v_a$) and 15. Let $(\hat{R}(t), \hat{b}(t))$ denote the solution of Eqn's 34-36. Assume that $\Omega(t)$ is a bounded, absolutely continuous signal that is persistently exciting and uncorrelated to the error signal $\tilde{R} = \hat{R}^T R$. Define

$$U_1 = \{(\tilde{R}, \tilde{b}) : v_{0a}^T \tilde{R} v_{0a} = -1, \tilde{b} = 0\}.$$

Then:

1. The set U_1 is forward invariant and unstable under the closed-loop filter dynamics.
2. The estimate $(\hat{v}_a, \hat{b})$ is locally exponentially stable to (v_a, b).
3. For almost all initial conditions $(\tilde{R}_0, \tilde{b}_0) \notin U_1$ then $(\hat{v}_a, \hat{b})$ converges to the trajectory $(v_a(t), b)$.

An important aspect of Corollary 2 is the convergence of the bias terms in all degrees of freedom. This ensures that (in the asymptotic limit) the drift in the attitude estimate around the unmeasured axis v_{0a} will be driven by a zero mean noise process rather than a constant bias term. In a practical setting, this makes the proposed filter a practical algorithm for most mAV applications.

7 Experimental results

In this section, we present experimental results to demonstrate the performance of the proposed observers.

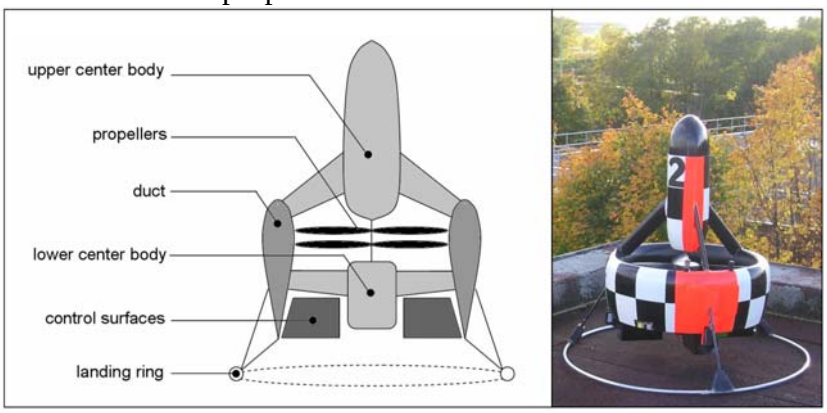

Fig. 7. The VTOL mAV HoverEye © of Bertin Technologies

Experiments were undertaken on two real platforms to demonstrate the convergence of the attitude and gyro bias estimates.

1. The first experiment was undertaken on a robotic manipulator with an IMU mounted on the end effector and sup-

plied with synthetic estimates of the magnetic field measurement. The robotic manipulator was programmed to simulate the movement of a flying vehicle in hovering flight regime. The filter estimates are compared to orientation measurements computed from the forward kinematics of the manipulator. Only the passive and direct complimentary filters were run on this test bed.

2. The second experiment was undertaken on the VTOL mAV HoverEye© developed by Bertin Technologies (Figure 7). The VTOL belongs to the class of 'sit on tail' ducted fan VTOL mAV, like the iSTAR9 and Kestrel developed respectively by Allied Aerospace [15] and Honeywell [10]. It was equipped with a low-cost IMU that consists of 3-axis accelerometers and 3-axis gyroscopes. Magnetometers were not integrated in the mAV due to perturbations caused by electrical motors. The explicit complementary filter was used in this experiment.

For both experiments the gains of the proposed filters were chosen to be: $k_P = 1\text{rd.s}^{-1}$ and $k_I = 0.3\text{rd.s}^{-1}$. The inertial data was acquired at rates of 25Hz for the first experiment and 50Hz for the second experiment. The quaternion version of the filters were implemented with first order Euler numerical integration followed by rescaling to preserve the unit norm condition.

Experimental results for the direct and passive versions of the filter are shown in Figures 8 and 9. In Figure 8 the only significant difference between the two responses lies in the initial transient responses. This is to be expected, since both filters will have the same theoretical asymptotic performance. In practice, however, the increased sensitivity of the direct filter to noise introduced in the computation of the measured rotation R_y is expected to contribute to slightly higher noise in this filter compared to the passive.

The response of the bias estimates is shown in Figure 9. Once again the asymptotic performance of the filters is similar after an initial transient. From this figure it is clear that the passive filter displays slightly less noise in the bias estimates than for the direct filter (note the different scales in the y-axis).

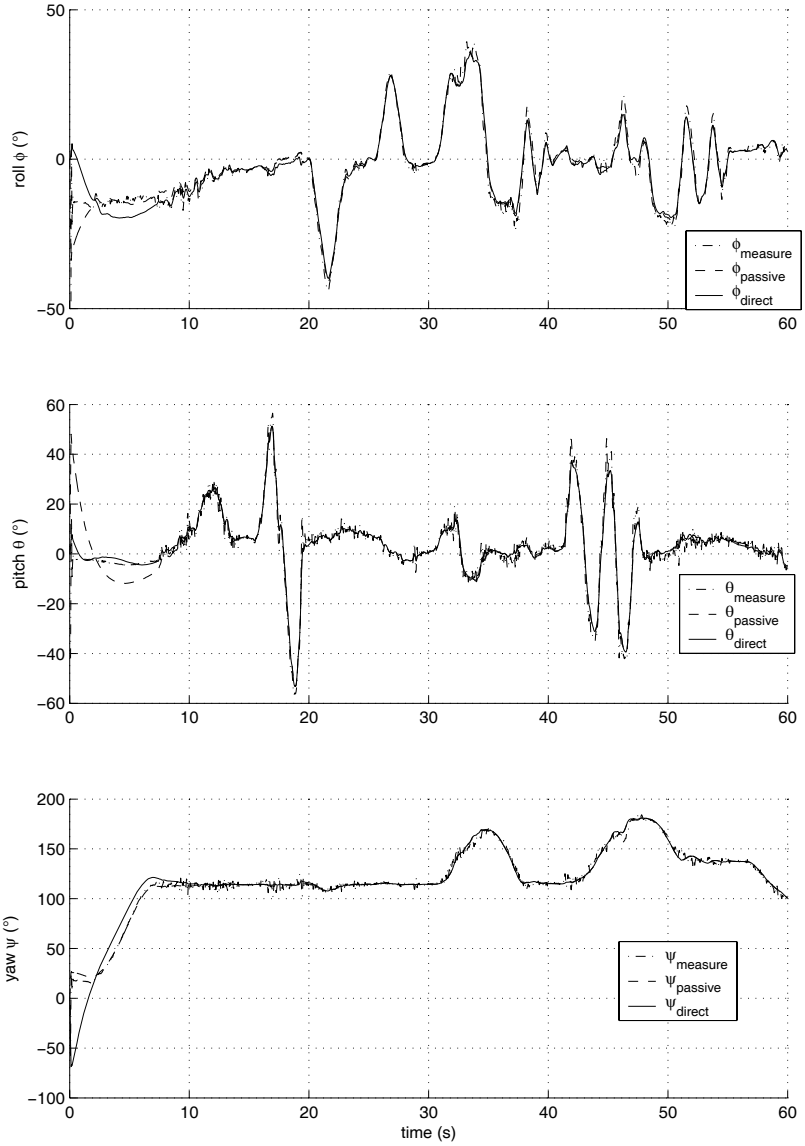

Fig. 8. Euler angles from direct and passive complementary filters

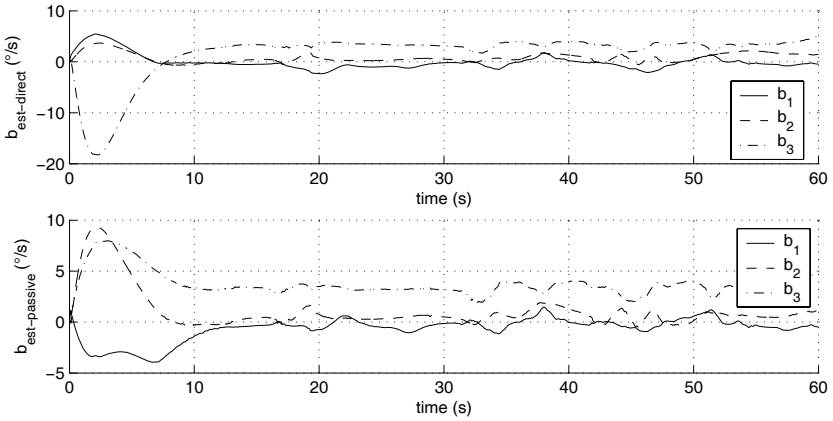

Fig. 9. Bias estimation from direct and passive complementary filters

Figures 10 and 11 relate to the second experiment. The experimental flight of the mAV was undertaken under remote control by an operator. The experimental flight plan used was: First, the vehicle was located on the ground, initially headed toward $\psi(0) = 0$. After take off, the vehicle was stabilized in hovering condition, around a fixed heading which remains close the initial heading of the vehicle on the ground. Then, the operator undertakes a $\Box 90^{\circ}$-left turn manoeuvre, returns to the initial heading, and follows with a $\Box 90^{\circ}$-right turn manoeuvre, before returning to the initial heading and landing the vehicle. After landing, the vehicle is placed by hand at its initial pose such that final and initial attitudes are the identical.

Figure 10 plots the pitch and roll angles (ϕ, θ) estimated directly from the accelerometer measurements against the estimated values from the explicit complementary filter. Note the large amounts of high frequency noise in the raw attitude estimates. The plots demonstrate that the filter is highly successful in reconstructing the pitch and roll estimates.

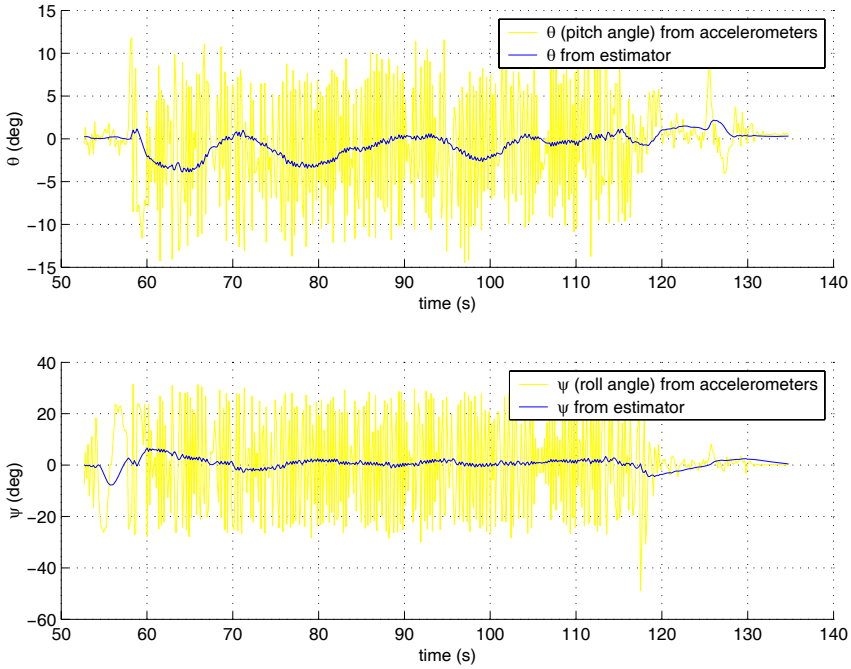

Fig. 10. Estimation results of the Pitch and roll angles

Figure 11 presents the gyros bias estimation verses the predicted yaw angle (ϕ) based on open loop integration of the gyroscopes. Note that the explicit complementary filter here is based solely on estimation of the gravitational direction. Consequently, the yaw angle is the indeterminate angle that is not directly stabilised in Corollary 2. Figure 11 demonstrates that the proposed filter has successfully identified the bias of the yaw axis gyro. The final error in yaw orientation of the microdrone after landing is less than 5 degrees over a two minute flight. Much of this error would be due to the initial transient when the bias estimate was converging. Note that the second part of the figure indicates that the bias estimates are not constant. Although some of this effect may be numerical, it is also to be expected that the gyro bias on low cost IMU systems are highly susceptible to vibration effects and changes in temperature. Under flight conditions changing engine speeds and aerodynamic conditions can cause quite fast changes in gyro bias.

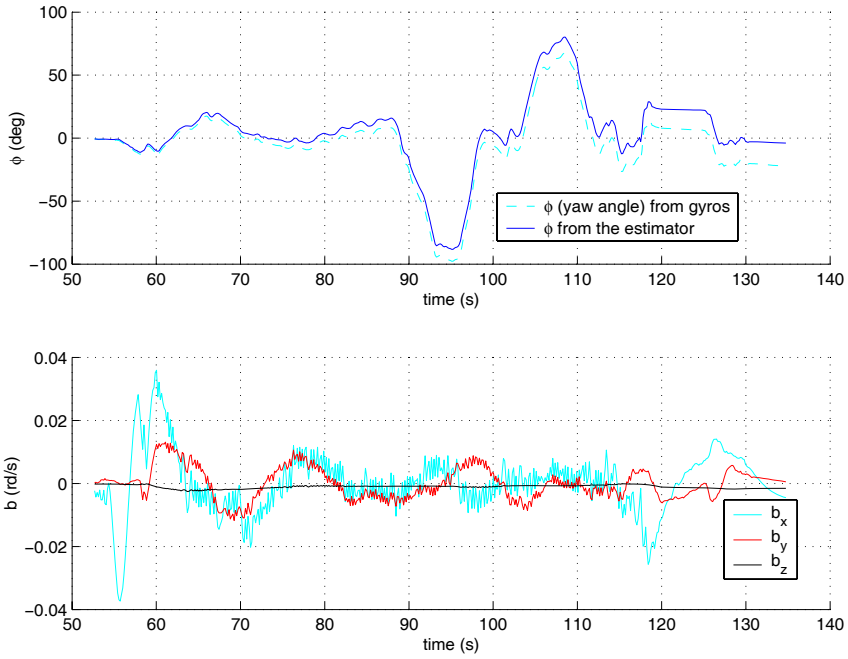

Fig. 11. Gyros bias estimation and influence of the observer on yaw angle.

8 Conclusions

This chapter presents a general analysis of attitude observer design posed directly on the special orthogonal group. Three non-linear observers are proposed:

Direct complementary filter: A non-linear observer posed on $SO(3)$ that is related to previously published non-linear observers derived using the quaternion representation of $SO(3)$.

Passive complementary filter: A non-linear filter equation that takes advantage of the symmetry of $SO(3)$ to avoid transformation of the predictive angular velocity term into the estimator frame of reference. The resulting observer kinematics are considerably simplified and avoid coupling of constructed attitude error into the predictive velocity update.

Explicit complementary filter: A reformulation of the passive complementary filter in terms of direct vectorial measurements, such

as gravitational or magnetic field directions obtained for an IMU. This observer does not require on-line algebraic reconstruction of attitude and is ideally suited for implementation on embedded hardware platforms. Moreover, the filter remains well conditioned in the case where only a single vector direction is measured.
The explicit complementary filter is now implemented as the primary attitude estimation system on several mAV vehicles world wide.

9 References

1 E.R. Bachmann, I. Duman, U.Y. Usta, R.B. McGhee, X.P. Yun, and M.J. Zyda. Orientation tracking for humans and robots using inertial sensors. In *Computational Intelligence in Robotics and Automation, 1999. CIRA '99. Proceedings. 1999 IEEE International Symposium on*, pages 187 – 194, Monterey,CA, USA., Nov 1999.

2 A-J. Baerveldt and R. Klang. A low-cost and low-weight attitude estimation system for an autonomous helicopter. *Intelligent Engineering Systems*, 1997.

3 B. Barshan and H.F. Durrant-Whyte. Inertial navigation systems for mobile robots. *IEEE Transactions on Robotics and Automation*, 44(4):751–760, 1995.

4 D.S. Bayard. Fast observers for spacecraft pointing control. In *Proceedings of the IEEE Conference on Decision and Control*, pages 4702–4707, Tampa, Florida, USA, 1998.

5 R. G. Brown and P. Y. C. Hwang. *Introduction to Random Signals and Applied Kalman Filtering*. John Wiley and Sons, New York, NY, 2nd edition, 1992.

6 P. Corke, J. Dias, M. Vincze, and J. Lobo. Integration of vision and inertial sensors. In *Proceedings of the IEEE International Conference on Robotics and Automation, ICRA '05.*, W-M04, Barcellona, Spain, April 2005. Full day Workshop.

7 Peter Corke. An inertial and visual sensing system for a small autonomous helicopter. *J. Robotic Systems*, 21(2):43–51, February 2004.

8 G. Creamer. Spacecraft attitude determination using gyros and quaternion measurements. *The Journal of Astronautical Sciences*, 44(3):357–371, July 1996.

9 Olaf Egland and J.M. Godhaven. Passivity-based adaptive attitude control of a rigid spacecraft. *IEEE Transactions on Automatic Control*, 39:842–846, April 1994.

10 J. Fleming, T. Jones, P. Gelhausen, and D. Enns. Improving control system effectiveness for ducted fan vtol uavs operating in crosswinds. In *Proc. of the 2nd "Unmanned Unlimited" System*, San Diego, USA, September 2003. AIAA.

11 T. Hamel and R. Mahony. Attitude estimation on $SO(3)$ based on direct inertial measurements. In *International Conference on Robotics and Automation, ICRA2006*, pages –, Orlando Fl., USA, April 2006. Institue of Electrical and Electronic Engineers.
12 M. Jun, S. Roumeliotis, and G. Sukhatme. State estimation of an autonomous helicopter using Kalman filtering. In *Proc. 1999 IEEE/RSJ International Conference on Robots and Systems (IROS 99)*, 1999.
13 Jong-Hyuk Kim and Salah Sukkarieh. Airborne simultaneous localisation and map building. In *Proceedings of the IEEE International Conference on Robotics and Automation*, pages 406–411, Taipei, Taiwan, September 2003.
14 E.J. Lefferts, F.L. Markley, and M.D. Shuster. Kalman filtering for spacecraft attitude estimation. *AIAA Journal of Guidance, Control and Navigation*, 5(5):417–429, September 1982.
15 L. Lipera, J.D. Colbourne, M.B. Tischler, M.Hossein Mansur, M.C. Rotkowitz, and P. Patangui. The micro craft istar micro-air vehicle: Control system design and testing. In *Proc. of the 57th Annual Forum of the American Helicopter Society*, pages 1–11, Washington DC, USA, May 2001.
16 J. Lobo and J. Dias. Vision and inertial sensor cooperation using gravity as a vertical reference. *IEEE Transactions on Pattern Analysis and Machine Intelligence*, 25(12):1597–1608, Dec. 2003.
17 Guang-Fu Ma and Xue-Yuan Jiang. Spacecraft attitude estimation from vector measurements using particle filter. In *Proceedings of the fourth Internation conference on Machine Learning and Cybernetics*, pages 682–687, Guangzhou, China, August 2005.
18 R. Mahony, T. Hamel, and J.-M. Pflimlin. Non-linear complementary filters on the special orthogonal group, 2006. 41 pages.
19 R. Mahony, T. Hamel, and Jean-Michel Pflimlin. Complimentary filter design on the special orthogonal group $SO(3)$. In *Proceedings of the IEEE Conference on Decision and Control, CDC05*, Seville, Spain, December 2005. Institue of Electrical and Electronic Engineers.
20 J.L. Marins, Xiaoping Yun, E.R. Bachmann, R.B. McGhee, and M.J. Zyda. An extended kalman filter for quaternion-based orientation estimation using marg sensors. In *Intelligent Robots and Systems, 2001. Proceedings. 2001 IEEE/RSJ International Conference on*, volume 4, pages 2003–2011vol.4, 29 Oct.-3 Nov. 2001.
21 N. Metni, J.-M. Pflimlin, T. Hamel, and P. Soueeres. Attitude and gyro bias estimation for a flying UAV. In *IEEE/RSJ International Conference on Intelligent Robots and Systems*, pages 295–301, August 2005.
22 N. Metni, J.-M. Pflimlin, T. Hamel, and P. Soueeres. Attitude and gyro bias estimation for a VTOL UAV. *Control Engineering Practice*, 14(12):1511–1520, December 2006.
23 J-P. Pflimlin, T.Hamel, P. Souères, and N. Metni. Nonlinear attitude and gyroscope's bias estimation for a VTOL UAV. In *Proceedings of the IFAC World Conference, IFAC2005*, 2005.

24 R.E. Phillips and G.T. Schmidt. *System Implications and Innovative Applications of Satellite Navigation*, volume 207 of *AGARD Lecture Series 207*, chapter GPS/INS Integration, pages 0.1–0.18. NASA Center for Aerospace Information, help@sti.nasa.gov, 1996.
25 H. Rehbinder and B.K. Ghosh. Pose estimation using line-based dynamic vision and inertial sensors. *IEEE Transactions on Automatic Control*, 48(2):186–199, Feb. 2003.
26 H. Rehbinder and X. Hu. Nonlinear state estimation for rigid body motion with low-pass sensors. *Systems and Control Letters*, 40(3):183–190, 2000.
27 Henrik Rehbinder and Xiaoming Hu. Drift-free attitude estimation for accelerated rigid bodies. *Automatica*, 4(4):Pages 653–659, April 2004.
28 J. Roberts, P. Corke, and G. Buskey. Low-cost flight control system for a small autonomous helicopter. In *Proceedings of the Australasian Conference on Robotics and Automation, ACRA02*, Auckland, New-Zealand, 2002.
29 S. Salcudean. A globally convergent angular velocity observer for rigid body motion. *IEEE Transactions on Automatic Control*, 46, no 12:1493–1497, 1991.
30 G. S. Sukhatme, G. Buskey, J. M. Roberts, P. I. Corke, and S. Saripalli. A tale of two helicopters. In *IEEE/RSJ, International Robots and Systems,*, pages 805–810, Los Vegas, USA, Oct. 2003. http://www-robotics.usc.edu/ srik/papers/iros2003.pdf.
31 A. Tayebi and S. McGilvray. Attitude stabilization of a vtol quadrotor aircraft. *IEEE Transactions on Control Systems Technology*, 14(3):562–571, May 2006.
32 J. Thienel and R. M. Sanner. A coupled nonlinear spacecraft attitude controller and observer with an unknow constant gyro bias and gyro noise. *IEEE Transactions on Automatic Control*, 48(11):2011 – 2015, Nov. 2003.
33 July Thienel. *Nonlinear observer/Controller dsigns for spacecraft attitude control systems with uncalibrated gyros*. Phd, Faculty of the Graduate School of the University of Maryland, Dep. Aerospace Engineering,, 2004.
34 B Vik and T. Fossen. A nonlinear observer for GPS and INS integration. In *Proceedings of the 40th IEEE Conference on Decision and Control*, 2001.
35 M. Zimmerman and W. Sulzer. High bandwidth orientation measurement and control based on complementary filtering. In *Proceedings of Symposium on Roboitcs and Control, SYROCO*, Vienna, Austria, 1991.